



Towards Low-Power Electronics: Self-Recovering and Flexible Gas Sensors

A. Falco,^a A. Rivadeneyra,^b F.C. Loghin,^b J.F. Salmeron,^b P. Lugli^a and A. Abdelhalim^b

Received 00th January 20xx,
Accepted 00th January 20xx

DOI: 10.1039/x0xx00000x

www.rsc.org/

New paradigm in recovery strategies for gas sensors is presented in this work. Resistive gas sensors based on carbon nanotubes (CNT) are well-known and show high sensitivity to different gas species but they require external recovery (i.e. heating) to offer a fast and stable response. In order to avoid this external element and reduce power demand, we demonstrate the possibility of recovering this kind of sensors by only applying a DC voltage. In particular, three different metals have been tested (Au, Ag and Al) to define interdigitated electrodes on a polyimide substrate. On top of them, CNT layers have been sprayed for the sensitive layer. The performance of these devices in terms of gas sensitivity, power consumption and stability is described and compared with external heating recovery. In particular, Au electrodes shows a response to 2500 ppm CO₂ of 2.6% with a recovery voltage of 5 V, presenting almost the same sensitivity as in the case of external recovery at 80 °C but decreasing the power demand more than 35 times.

Introduction

The importance of gas sensor is undeniable as they play a fundamental role in industrial emission, environmental pollution, medical diagnosis, food processing, among others^{1,2}. For example, the monitoring of CO₂ is necessary, among other reasons, to optimally control of indoor air quality (IAQ)^{3,4}. In the case of NH₃, its control is important in industrial, medical, and living environments⁵. There have been many efforts to develop this kind of devices from traditional techniques; such as gas chromatography (GC), also coupled to mass spectrometry or atomic emission detection; to new trends based on functional sensing materials. One quite used solution is sensors based on optical absorption, such as CO₂ sensors^{6,7}. This approach offer fast responses, minimal drift and high gas specificity, with zero cross response to other gases as long as their design is carefully considered⁸. Although the traditional techniques present high sensitivity, accuracy and reliability, they are time consuming and power demanding as well as high maintenance requirement^{9,10}.

Different approaches have been developed towards facing these issues, for instance, higher-order sensing systems which consist of sensor arrays covered with different sensitive layers^{11,12}, using pattern recognition algorithms¹³ or multifunctional sensors which measure different properties of a sensitive layer^{14,15}. In this sense, functional materials have received a lot of attention. There are a large variety of electrical sensor

materials, including semiconducting metal oxides^{5,16}, silicon devices^{17,18}, organic materials^{19,20}, and carbon black–polymer composites²¹. For instance, semiconducting metal oxides have been extensively used for NO₂ and NH₃ monitoring^{5,16,22}. These sensors operate at high temperatures (200 to 600 °C) in order to enhance the chemical reactivity between molecules and sensing layer for significant sensor response²². Recently, researches have focused their interests on carbon nanotubes (CNTs) for their attractive features, such as chemical, thermal and mechanical stability, metallic and semi conductive properties⁹. CNTs have been extensively used to manufacture gas sensors based on resistive changes^{23–28}, showing good sensor response to a wide range of gases and volatile organic compounds.

Among the sensor characteristics, the time response is a crucial aspect that is desired to be as fast as possible, meaning that the sensor can be quickly recovered over time. A common strategy to achieve this fast response on resistive gas sensors is to heat their active layer forcing the trapped molecules to escape^{29–36}. The drawback of this approach is the increase in power consumption as well the increasing cost of the heating element. Some authors have already investigated other approaches to optimize the recovery of CNT-based sensors. For example, Sharma et al. combined conventional thermal treatment with DC voltage bias³⁷. Other strategies analysed are ultraviolet (UV) light exposure^{38,39} or applying current pulse⁴⁰. In this work, we present a novel and innovative technique – self-recovery – to recover CNT-based gas sensors without using any external recovery element. Such technique utilizes the CNT layer as sensing layer for gas detection as well as heating layer for sensor recovery. Exploding the heating properties of this sensing layer, the recovery of the gas sensor is obtained by applying voltage directly to the sensory structure without any external element, reducing the number of devices in a final system and

^a Address here.

^b Address here.

^c Address here.

† Footnotes relating to the title and/or authors should appear here.

Electronic Supplementary Information (ESI) available: [details of any supplementary information available should be included here]. See DOI: 10.1039/x0xx00000x

simultaneously decreasing the power consumption because no high voltages are required to activate this phenomenon. In order to present the self-recovery concept, we characterized the heating capabilities of the sensor in terms of reached temperature, applied voltage and consumed power. Different metals (Au, Ag and Al) were used as electrodes. For instance, Ag-based devices reached a temperature of 120 °C at 30 V bias, while Al-based devices resulted in a very high resistive CNT, which subsequently hindered the heating functionality. We described the self-recovery concept in the functionality of the gas sensor and compared its performance to the case of recovering by external heating. The technique developed here optimizes the performance of CNT-based gas sensor. But it also paves the way towards ultralow power, stable and cost-effective flexible electronics.

Device fabrication and characterization

The chosen substrates were a polyimide (Kapton HN) with a thickness of 125 μm . An interdigitated electrode structure (IDES) consisting of a 50-nm metal layer was evaporated on top of the polyimide with a width and distance between two consecutive fingers of 100 μm , occupying a total area of 9 mm^2 . Three different metals were tested: Au, Ag and Al.

The CNT solution was dispersed in an aqueous solution based on sodium dodecyl sulfate (SDS) following the procedure described we reported in previous works⁴¹. The deposition of the CNT solution was performed through an automated spray deposition system equipped with a commercially available air atomizing spray valve (Nordson EFD, USA) mounted on motorized platform (Precision Valve & Automation, USA). The most important parameters to be adjusted to fine tune the characteristics of the final result were set using an approach similar to what previously reported^{42, 43}.

In order to examine the self-recovery property of the fabricated CNT-based devices, a 3D printed module was built for in-situ temperature monitoring. In this module shown in Figure 1, the CNT device is placed on top of a Pt100 sensor which is located in a groove in the carrier part. The sensor is fixed on the carrier part by a lid with an opening in the middle to allow contacting the sensor. Regarding the gas characterization, we used the same procedure previously reported in²⁵. In particular, we employed a benchtop impedance analyser (Keysight E4990A) to measure the impedance and apply – when needed – a DC bias. The real part of the impedance measured at 20 Hz was employed as an approximation of the DC resistance in the following sections.

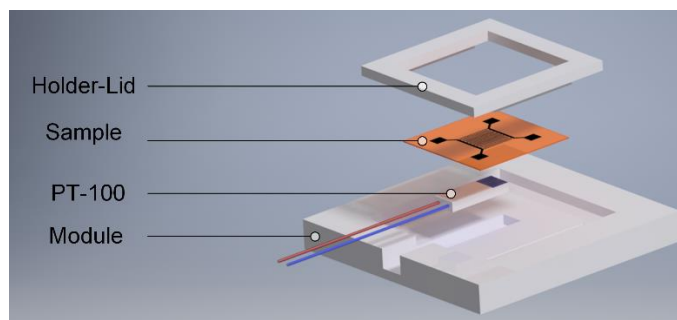


Figure 1. Schematic for the 3D printed module used in characterizing the self-recovery property of the CNT-based gas sensor.

Results and discussion

First, the IV curves of the different fabricated devices are studied to outline the self-recovery working principle. Using this information, the heating properties of the best candidates are described, highlighting the physical phenomenon behind this property. Finally, once the heating properties are demonstrated, we present the gas sensor working under self-recovery regime, emphasizing its features with respect to other similar sensors with different recovery strategies.

A. IV Curve

As a starting point for the understanding of the working principle of these devices, IV characteristics have been recorded (Figures 2a and 2b), as this kind of measurement gives excellent indications of the linearity of the system and its operational limits. The initial resistance (i.e. the slope around 0 V) of the combination of CNT films with the different metal electrodes diverges significantly, ranging from 1.4 $\text{k}\Omega$ to 2.8 $\text{k}\Omega$ for Ag, from 3.6 $\text{k}\Omega$ to 8.0 $\text{k}\Omega$ for Au, from 28.9 $\text{k}\Omega$ to 125.6 $\text{k}\Omega$ for Al.

Since the tube density and the deposition process parameters were kept constant for each sample, the intrinsic resistance of the CNT networks is to be considered a constant of the CNT/electrode system. As a consequence, the change in resistance is to be attributed to the different contact resistances between the metals and the CNTs and to the formation of a Schottky barrier due to the difference between the Fermi Level of the CNTs and the work function of the metals⁴⁴⁻⁴⁶. Furthermore, since the whole processing is conducted in a non-inert atmosphere, the absorption of water and oxygen on the surface of the metals prior to the CNT deposition cannot be avoided and this could lead to the formation of a surface dipole⁴⁴. The proposed band structures are depicted in Figure S1 (Supporting information), showing how the creation of a surface dipole might lead to the mitigation of the Schottky barrier at the Ag/CNTs interface and to the increase of the ohmic barrier at the Au/CNTs interface.

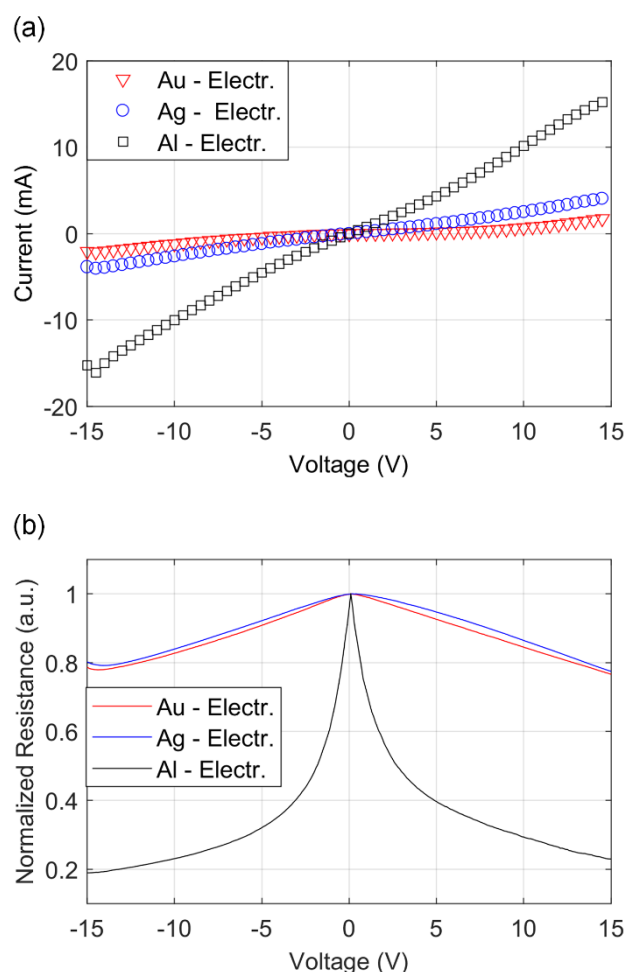


Figure 2. (a) Current vs. voltage curve (a) and normalized resistance vs. voltage (b) for the different metal electrodes, Au (red), Ag (blue) and Al (black).

The insurgence of these phenomena justifies the linearity of the IV curves for Au and Ag electrodes and, at the same time, the higher resistance of the Au-based devices with respect to the Ag-based ones. Figure 2b illustrates the evaluated point-wise resistance (defined as the ratio of the applied voltage to the measured current) of the different devices which highlights the strong non-linearity of the Al-based devices. The resistance is subject to a sudden change with increasing voltage and it is reduced to 30% of its initial value when 5 V are applied, moving to a more linear regime, suggesting that the potential barrier is finally overcome.

B. Heater Characterization

In this section, we develop the self-recovery concept of CNTs as the first step towards its successful employment in the operation of CNT-based gas sensors. We performed several characterization schemes to investigate the device limits in terms of temperature, voltage and power. The concept of self-recovery can be explained as follow, applying DC voltage to the CNT thin-film, which is deposited on top of an IDE structure, results in high current density in the single nanotubes (NTs) that generates heat energy. The amount of current passing through the CNT network depends mainly on the resistance of the

network, which is –as discussed earlier- highly influenced by the IDEs material and the contact between this material (metal) and the CNT network. In that context, we applied voltage in increasing steps of 5 V from 0 V to 30 V (forward), and then decreased it again till 0 V (backward). Al-based devices were excluded due to their high resistance that hindered the heating function. Figure 3 shows the relation between the voltage and the temperature for Au-(red) and Ag-(blue) based devices, while the inset picture shows a thermal image for the device when voltage is applied. One can notice that Ag-based devices can reach almost 120 °C under 30 V, while the maximum reached by Au-based devices was only 72 °C, given the same CNT density. This difference is mainly attributed to the high conductance of Ag-based sensors, which is associated to the lower Schottky barrier formed between the semiconducting carbon nanotubes (SC-CNT) and the metal electrodes, as explained in the previous section.

We can observe as well that the forward path and the backward path do not coincide, which indicates that the resistance changes because of the generated heat in the CNT layer not having enough time to recover the ambient conditions. We have reported previously⁴⁷ the change that occurs in the resistance of the CNT layer under different operating temperatures. We performed further investigation on such relation by varying the voltage rather than the temperature (shown in Figure S2a, Supporting information). Briefly, heating up the CNT layer, either by applying external heat or by applying voltage -so the heat is internally generated- produces change and instability in the layer's resistance. This variation could be reversible if the heat energy is below certain threshold, otherwise it is irreversible^{48, 49}.

On the one side, while operating below the threshold value, the procedure of heating up and cooling down the CNT layer will result in a pre-defined variation for the resistance that will occur each time that such procedure is repeated, as shown in Figure S2b (Supporting information).

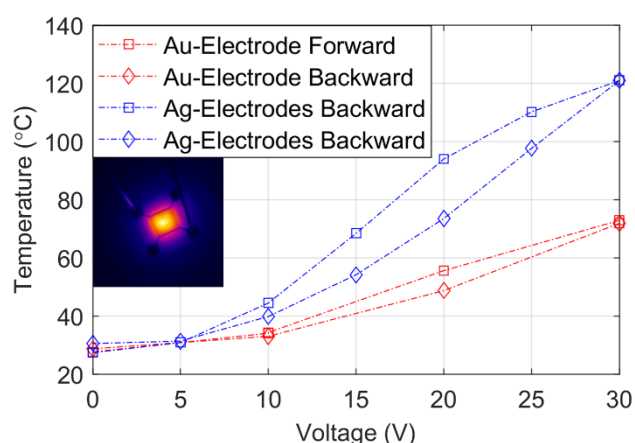


Figure 3. Relation between voltage and temperature for Au- (red) and Ag- (blue) based devices. Forward and backward lines represent the increase and decrease in voltage, respectively. Inset picture is a thermal image for a CNT-based gas sensor under bias.

On the other side, when operating in a regime higher than this threshold, the resistance finds a new 'stable' point. Moreover, in such regime each time the procedure is repeated, the threshold value itself changes and shifts to a higher value, as depicted in Figure S2c (Supporting information).

In general, the behavior of the resistance with respect to the temperature/applied voltage is influenced by several factors, such as density of the CNT layer, electrodes material and subsequently the initial resistance of the film.

While operating at temperatures below 50°C, the heating throughout the sample is spatially uniform, as confirmed by thermal camera investigations (see inset of Figure 3), and mostly confined to the area covered by the interdigitated electrodes. However, although the macroscopic temperature distribution is flat and associated with a big central hot-spot, a similar analysis performed at micro- or nano-scale yields different results. The combination of the high thermal conductivity of CNTs and the insulating behavior of the polymeric sample creates a strong temperature gradient between the areas covered by the CNT network and the uncovered ones. To gain a better insight in this phenomenon, thermodynamic simulations of a simplified system were carried out with a commercial multiphysics environment (COMSOL Multiphysics 5.0).

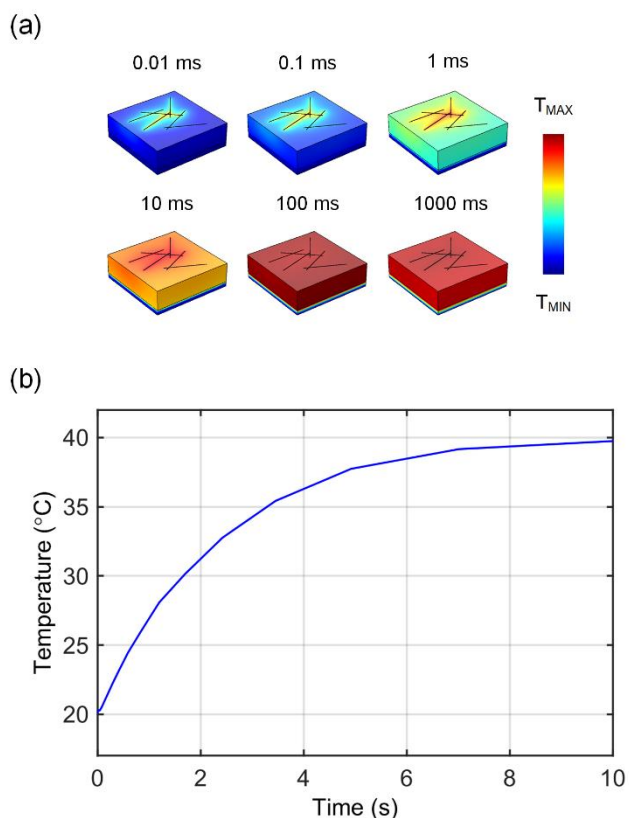


Figure 4. COMSOL simulation of a network made of six CNTs upon the application of a 0.1 V voltage at the extremes. The top panels (a) show the temperature distribution in different instants. The bottom panel (b) shows the temperature of the bottom side of the substrate. The CNT density ($6 \text{ CNTs}/\mu\text{m}^2$) is comparable to the average CNT density of the fabricated sensors, while the applied voltage, if linearly scaled up to a $100 \mu\text{m}$ wide structure, are equivalent to 10 V.

The considered system is composed of six interconnected carbon nanotubes subjected to a voltage applied between the left and the right side of the domain. The voltage induces a current in the tubes and leads to a concentrated heat dissipation in few microseconds (Figure 4 (a)), and the temperature then diffuses on a milliseconds time-scale to the complete surface around the CNTs. The simulation takes into account the thermoelectric heating of the tubes, the different thermal conductivity on the two axes of the tubes, and a cooling effect due to air convection from a flat horizontal plate.

Figure 4b, shows how consistently with our macroscopic characterizations, the thermal steady state is reached within few seconds from the start of the heating process. The plot shows the temporal evolution of temperature at the bottom side of the substrate upon the application of a small voltage to the terminals. The phenomenon of immediate local rise of temperature in the CNT and slow diffusion to the remaining sample, however, cannot be captured by macroscopic characterization. The local heating, however, is key to the understanding of the self-recovering behavior of the gas sensors presented in this contribution, and its main advantages.

C. Gas Sensor characterization

Heaters, in general, are essential in the operation of gas sensors⁵⁰. For CNT-based gas sensors, heaters are used to actively recover the sensor after exposure intervals. We have previously reported the difference between active recovery and passive recovery for these sensors²⁶. In that context, a Peltier element or micro heaters are commonly used to heat up the CNT layer up to certain temperature after each exposure cycle. Such heating process helps in a faster desorption of the attached molecules to the surface of the CNTs. On the contrary, passive recovery is performed at room temperature but requires longer waiting time to achieve the full recovery of the sensor.

Using the self-recovery concept instead of any external heating technique decreases not only the power consumed by the sensor but also the whole manufacturing cost of the device. Furthermore this strategy facilitates its integration in a more complex system.

As previously reported, the active recovery is the process of supplying enough energy to the single NTs in order to overcome the desorption barrier and release the adsorbed molecules²⁶. Supplying this energy by external means produces also partial heat dissipation as well as diffusion in the surroundings. Thus, the application of a recovery temperature (i.e. 80 °C) to the substrate results in a certainly lower local temperature at the nanotube. Consequently, a procedure similar to active recovery can be attained at lower local temperature if the CNT layer itself is the supplier of the heat energy, being more energy-efficient and effective. We will refer to this mechanism as internal heating or, more properly, as "self-recovery". In fact, although, as presented in the previous section, the high current densities in the film yield a localized temperature rise, they are also associated to non-thermal processes, which contribute to the gas desorption from the film. As thoroughly described by Salehi-Khojin et al.⁵¹, under certain circumstances, the gas desorption

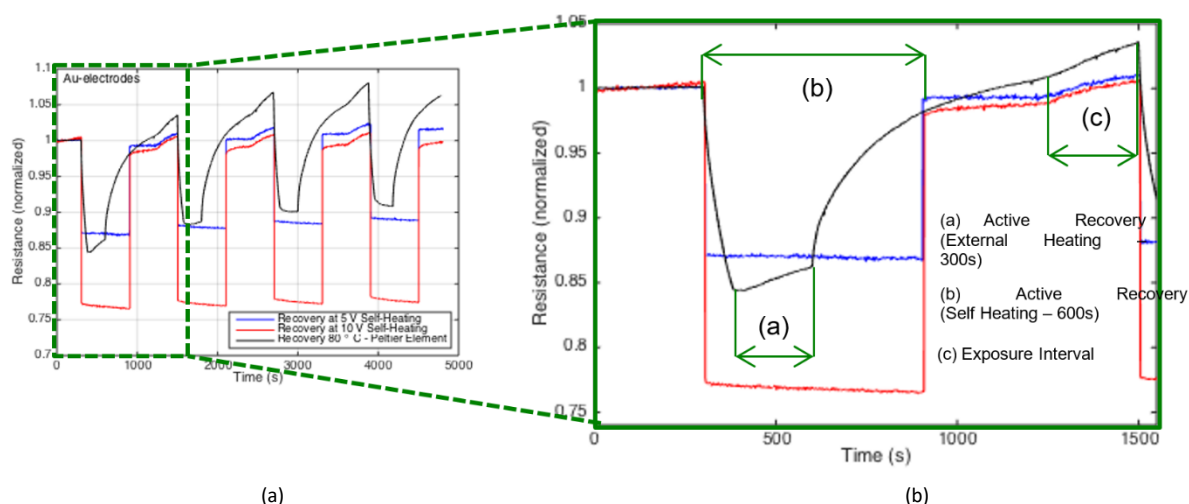


Figure 5. Time vs. resistance for Au-CNT-based gas sensor exposed for three times with 2500 ppm of CO₂. Three different recovery techniques were performed, bias of 5 V (blue), bias of 10 V (red) and external heating at 80 °C (black).

is incremented by hot carriers flowing through the defects with a Poole-Frenkel conduction mechanism. Differently from this previous report, however, where no thermal effect was detected, we observe that internal heating and Poole-Frenkel conduction act synergically to the complete recovery of the sensor.

To prove the validity of self-recovery of gas sensors, CNT-based gas sensors were exposed to 2500 ppm of CO₂ with an exposure interval of 300 s, as illustrated in Figure 5. One cycle consists of an exposure interval followed by a recovery stage. A periodic cycle – consisting of active recovery, settling time and exposure time – has a total duration of 1200 s. Each cycle is repeated three times. The black curve indicates performing the active recovery for 300 s using a Peltier element, followed by a 300 s interval deemed necessary to let the sensor return to room temperature. The blue and the red curves indicate performing self-heating recovery by applying 5 V and 10 V to the CNT layer, respectively. Since recovering an Au-based device at these voltages does not induce any significant heating to the substrate, it is not necessary to let the sensor cool down for 300 s. Hence, to have easier comparison between the different methods, the recovery bias was kept for 600 s, preserving the overall 1200 s long periodic cycle. Looking at the plots, we can observe that recovery through external heating (black curve) shows the highest drift in the resistance baseline. This can be related to the behavior of the resistance with respect to the applied temperature, as discussed earlier. Such drift indicates that 80 °C is around the threshold temperature value for this CNT density, which subsequently gives a new layer resistance each time this value is reached. Moreover, the sensor presents a slow recovery from the resistance change induced by the heating process. After 600 s, when the exposure starts again, the resistance is still slowly increasing. Conversely, upon the application of 5 V (blue curve) we observe a much more limited baseline drift and no noticeable change in resistance when the bias is removed. The former effect can be attributed to the partial recovery of the sensor. The heat generated in the CNT

layer due to such voltage is not enough to desorb all the attached CO₂ molecules, and the Poole-Frenkel conduction alone is not able to guarantee a full and immediate desorption. However by applying 10 V (red curve) to recover the sensor, the measurement shows almost no baseline drift. In a classical Poole-Frenkel model⁵², the conduction of hot electrons is assisted by increased thermal energy. The application of higher voltages, contemporaneously yields higher electric fields and an increase in temperature. The two combined effects render the tunneling through defect states much more likely and result in a complete desorption of the gas. It is worth mentioning here that in order to keep the discussion comparable to most of the related articles in literature, the discussion in this section focuses on the Au-based devices. The measurements performed on Ag-based devices are presented in the supporting information.

Previously, we reported that the performance of the sensor decreases when it is exposed to the test gas at elevated temperature rather than room temperature²⁶. This is attributed to the fact that at elevated temperature, the desorption rate is relatively high which results in less molecules attaching to the CNT layer. In that context, we performed similar experiment where CNT-based gas sensor is exposed to CO₂ at certain bias rather than 0 V. For direct comparison, we performed the experiment as well by varying the operating temperature by means of external heating. Such measurement helps in better understanding of the self-recovery concept operation. Additionally, it serves as further confirmation of its efficiency over other commonly used techniques.

Figure 6 shows one cycle, where CNT-based gas sensor is exposed to 2500 ppm of CO₂ at different operating Conditions. In Figure 6a the exposure interval is performed at 0 V (blue curve), 1 V (red curve) and 4 V (black curve), while the recovery in the three cases is performed at 5 V. The choice of 5 V over 10 V for the recovery phase was taken to avoid unintentional substrate heating and to reduce the energy consumption of the sensor. In Figure 6b, the exposure interval is performed at 30 °C

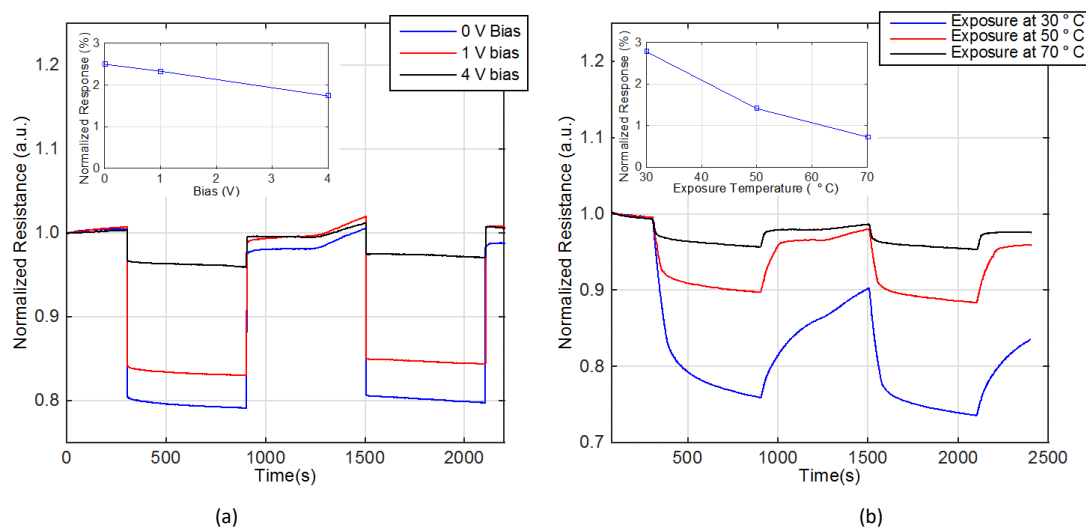


Figure 6. Time vs. resistance for Au-CNT-based gas sensors exposed to 2500 ppm of CO₂ under different operating conditions, different bias (a) and different temperature (b). In (a) the sensor is recovered by applying 5 V, while in (b), the sensor is recovered by external heating up to 80 °C. The inset pictures represent the relation between the normalized response and the operating conditions used in each plot.

(blue curve), 50 °C (red curve) and 70 °C (black curve), while the recovery in the three cases is performed at 80 °C. The inset pictures represent the relation between the normalized response and the corresponding exposure conditions. It is worth mentioning here that the normalized response is defined as:

$$\text{Normalized Response} = \frac{R_f - R_i}{R_i} \quad (1)$$

where R_i and R_f represents the initial and the final resistance value at the exposure interval, respectively. Moreover, it is important to notice how, in Figure 6a, each plot line is normalized to its initial value under bias, namely 1.50 k Ω , 1.45 k Ω and 1.30 k Ω , for 0 V, 1 V and 4 V, respectively. In self-recovery condition (5 V) the resistance of the device was almost constant for each cycle, to a value of circa 1.2 k Ω .

Exposing the sensor to the test gas at certain bias resulted -as expected- in lower normalized response when compared to the value obtained at zero bias. Nevertheless, the decrease in the normalized response when different biases are applied is not as much as the change occurs due to external heating. Quantitatively, the normalized response dropped from 2.6% at 0 V to 1.9% at 4 V. On the other hand, it dropped from 2.8% at 30 °C to 0.9% at 70 °C. This implies that the effect of applying 4 V is less than the effect of 70 °C in terms of energy supplied to the CNT layer. Such results agree with the plot in Figure 3, which shows that reaching 70 °C requires applying at least 30 V to the CNT layer. Similar to Figure 4, active recovery by means of external heating resulted in drift in the baseline resistance. Such behavior can be avoided by employing the self-recovery concept.

As already mentioned, one of the main advantages of this new recovery strategy is the drastic reduction of the power required to drive any external heating element. In this sense, power requirements for external heating at 80 °C is about 500 mW

whereas self-recovery consumes only about 64 mW at 10 V and 14 mW at 5 V. Therefore, the power saving with self-recovering is more than 7 times at 10 V and more than 35 times at 5 V with respect to external heating approach, leading to a more efficient approach.

Conclusions

Gas sensors based on CNTs layers show a very slow time response limiting their use in environments with fast variations in gas concentration. To improve their performance, external heat is applied to accelerate the desorption of the gas molecule trapped in the CNT network. This strategy penalizes the power consumption of the final system because temperatures above 80 °C are normally required to enhance the time response. We prove in this work how this kind of sensor can be self-recovered by applying low voltage between its terminals. In particular, with this self-recovery mechanism, the sensitivity towards CO₂ of a CNT-based gas sensor with Au electrodes is the same achievable with external heating. The unvaried sensitivity is accompanied by a reduction in the power consumption of more than 30 times and by the virtual elimination of resistance drift in the CNT sensor. This strategy opens new possibilities in gas sensor design, reducing the power requirement, the electronic components needed to drive the sensors and the overall sensor stability.

Conflicts of interest

There are no conflicts to declare.

Acknowledgements

Research supported by the TUM-Graduate School.

References

1. N. Yamazoe, *Sensors and Actuators B: Chemical*, 2005, **108**, 2-14.
2. E. Contés-de Jesús, J. Li and C. R. Cabrera, 2013.
3. S.-F. Ferng and L. Li-Wen, *Journal of Environmental Health*, 2002, **65**, 14.
4. J. M. Daisey, W. J. Angell and M. G. Apte, *Indoor air*, 2003, **13**, 53-64.
5. Y. Takao, K. Miyazaki, Y. Shimizu and M. Egashira, *Journal of the Electrochemical Society*, 1994, **141**, 1028-1034.
6. Z. Zhujun and W. R. Seitz, *Analytica chimica acta*, 1984, **160**, 305-309.
7. X. Ge, Y. Kostov and G. Rao, *Biotechnology and bioengineering*, 2005, **89**, 329-334.
8. J. Hodgkinson and R. P. Tatam, *Measurement Science and Technology*, 2013, **24**, 012004.
9. S. Niyogi, M. Hamon, H. Hu, B. Zhao, P. Bhowmik, R. Sen, M. Itkis and R. Haddon, *Accounts of Chemical Research*, 2002, **35**, 1105-1113.
10. X. Liu, S. Cheng, H. Liu, S. Hu, D. Zhang and H. Ning, *Sensors*, 2012, **12**, 9635-9665.
11. C. Hagleitner, A. Hierlemann, D. Lange, A. Kummer, N. Kerness, O. Brand and H. Baltes, *Nature*, 2001, **414**, 293-296.
12. C.-P. Chang and C.-L. Yuan, *Journal of materials science*, 2009, **44**, 5485-5493.
13. F. Hossein-Babaei, S. Hosseini-Golgoo and A. Amini, *Sensors and Actuators B: Chemical*, 2009, **142**, 19-27.
14. J. Covington, S. Tan, J. Gardner, A. Hamilton, T. Koickal and T. Pearce, 2003.
15. J.-J. Su, L. Beardslee and O. Brand, 2013.
16. Y. Shimizu and M. Egashira, *Mrs Bulletin*, 1999, **24**, 18-24.
17. H. McConnell, J. Owicki, J. Parce, D. Miller, G. T. Baxter, H. Wada and S. Pitchford, *Science*, 1992, **257**, 1906-1912.
18. A. Mandelis and C. Christofides, *Physics, chemistry and technology of solid state gas sensor devices*, John Wiley & Sons, 1993.
19. J. J. Miasik, A. Hooper and B. C. Tofield, *Journal of the Chemical Society, Faraday Transactions 1: Physical Chemistry in Condensed Phases*, 1986, **82**, 1117-1126.
20. S. Capone, S. Mongelli, R. Rella, P. Siciliano and L. Valli, *Langmuir*, 1999, **15**, 1748-1753.
21. M. C. Lonergan, E. J. Severin, B. J. Doleman, S. A. Beaber, R. H. Grubbs and N. S. Lewis, *Chemistry of Materials*, 1996, **8**, 2298-2312.
22. *Special issue on Gas-Sensing Materials*, MRS Bull, 1999.
23. L. Valentini, C. Cantalini, I. Armentano, J. Kenny, L. Lozzi and S. Santucci, *Diamond and Related Materials*, 2004, **13**, 1301-1305.
24. R. Ionescu, E. Espinosa, E. Sotter, E. Llobet, X. Vilanova, X. Correig, A. Felten, C. Bittencourt, G. Van Lier and J.-C. Charlier, *Sensors and Actuators B: Chemical*, 2006, **113**, 36-46.
25. A. Abdellah, A. Abdelhalim, F. Loghin, P. Kohler, Z. Ahmad, G. Scarpa and P. Lugli, *Sensors Journal, IEEE*, 2013, **13**, 4014-4021.
26. A. Abdellah, A. Abdelhalim, M. Horn, G. Scarpa and P. Lugli, *Nanotechnology, IEEE Transactions on*, 2013, **12**, 174-181.
27. A. Abdelhalim, M. Winkler, F. Loghin, C. Zeiser, P. Lugli and A. Abdellah, *Sensors and Actuators B: Chemical*, 2015, **220**, 1288-1296.
28. C. Piloto, F. Mirri, E. A. Bengio, M. Notarianni, B. Gupta, M. Shafiei, M. Pasquali and N. Motta, *Sensors and Actuators B: Chemical*, 2016, **227**, 128-134.
29. D. Vincenzi, M. Butturi, V. Guidi, M. Carotta, G. Martinelli, V. Guarnieri, S. Brida, B. Margesin, F. Giacomozzi and M. Zen, *Sensors and Actuators B: Chemical*, 2001, **77**, 95-99.
30. K. Crowley, A. Morrin, A. Hernandez, E. O'Malley, P. G. Whitten, G. G. Wallace, M. R. Smyth and A. J. Killard, *Talanta*, 2008, **77**, 710-717.
31. S. Claramunt, O. Monereo, M. Boix, R. Leghrib, J. Prades, A. Cornet, P. Merino, C. Merino and A. Cirera, *Sensors and Actuators B: Chemical*, 2013, **187**, 401-406.
32. M. Camara, F. Molina-Lopez, E. Danesh, G. Mattana, A. Bontempi, D. Teyssieux, L. Thiery, P. Breuil, C. Pijolat and K. Persaud, 2013.
33. G. P. Evans, D. J. Buckley, N. T. Skipper and I. P. Parkin, *RSC Advances*, 2014, **4**, 51395-51403.
34. E. Danesh, F. Molina-Lopez, M. Camara, A. Bontempi, A. s. V. s. Quintero, D. Teyssieux, L. Thiery, D. Briand, N. F. De Rooij and K. C. Persaud, *Analytical chemistry*, 2014, **86**, 8951-8958.
35. M. Rieu, M. Camara, G. Tournier, J. Viricelle, C. Pijolat, N. de Rooij and D. Briand, *Procedia Engineering*, 2015, **120**, 75-78.
36. J. Ramírez, F. Annanouch, M. Camara, E. Llobet and D. Briand, *Procedia Engineering*, 2015, **120**, 707-710.
37. S. Sharma, S. Hussain, S. Singh and S. Islam, *Sensors and Actuators B: Chemical*, 2014, **194**, 213-219.
38. Y. Hu, J. Zhou, P. H. Yeh, Z. Li, T. Y. Wei and Z. L. Wang, *Advanced Materials*, 2010, **22**, 3327-3332.
39. J. Li, Y. Lu, Q. Ye, M. Cinke, J. Han and M. Meyyappan, *Nano Letters*, 2003, **3**, 929-933.
40. C. Huang, B. Huang, Y. Jang, M. Tsai and C. Yeh, *Diamond and related materials*, 2005, **14**, 1872-1875.
41. A. Falco, L. Cinà, G. Scarpa, P. Lugli and A. Abdellah, *ACS applied materials & interfaces*, 2014, **6**, 10593-10601.
42. A. Abdellah, B. Fabel, P. Lugli and G. Scarpa, *Organic Electronics*, 2010, **11**, 1031-1038.
43. A. Abdelhalim, A. Abdellah, G. Scarpa and P. Lugli, *Carbon*, 2013, **61**, 72-79.
44. J. Svensson and E. E. Campbell, *Journal of applied physics*, 2011, **110**, 111101.
45. X. Cui, M. Freitag, R. Martel, L. Brus and P. Avouris, *Nano Letters*, 2003, **3**, 783-787.
46. C. Cao, J. B. Andrews, A. Kumar and A. D. Franklin, *ACS nano*, 2016.
47. S. Colasanti, V. D. Bhatt, A. Abdelhalim and P. Lugli, *IEEE Transactions on Electron Devices*, 2016, **63**, 1346-1351.
48. E. Cagatay, A. Falco, A. Abdellah and P. Lugli, 2014.
49. S. Colasanti, V. Robbiano, F. C. Loghin, A. Abdelhalim, V. D. Bhatt, A. Abdellah, F. Cacialli and P. Lugli, *IEEE Transactions on Nanotechnology*, 2016, **15**, 171-178.
50. I. Simon, N. Bârsan, M. Bauer and U. Weimar, *Sensors and Actuators B: Chemical*, 2001, **73**, 1-26.
51. A. Salehi-Khojin, K. Y. Lin, C. R. Field and R. I. Masel, *Science*, 2010, **329**, 1327-1330.
52. J. Simmons, *Journal of Physics D: Applied Physics*, 1971, **4**, 613.